

Nucleon and Δ isobar in a strong magnetic field

Ulugbek Yakhshiev,^{1,*} Hyun-Chul Kim,^{1,2,3,†} and Makoto Oka^{2,‡}

¹*Department of Physics, Inha University, Incheon 22212, Republic of Korea*

²*Advanced Science Research Center, Japan Atomic Energy Agency, Shirakata, Tokai, Ibaraki, 319-1195, Japan*

³*School of Physics, Korea Institute for Advanced Study (KIAS), Seoul 02455, Republic of Korea*

(Dated: February 4, 2019)

We investigate the static properties of the nucleon in the presence of strong magnetic fields and discuss the consequent changes of the nucleon structure, based on the Skyrme model. The results show that at large values of the magnetic field ($\sim 10^{17}$ to 10^{18} G), which is supposed to appear in heavy-ion collision experiments at RHIC energies, the soliton starts to deviate from the spherically symmetric form and its size starts to change. At extremely large values of the magnetic field ($\sim 10^{19}$ G), which may be found at the LHC experiments, the soliton becomes more compact than in free space. The results also show that in the presence of the external magnetic field, the mass of the nucleon tends to increase in general and the mass degeneracy of the Δ isobars from isospin symmetry will be lifted. We also discuss the changes in the mass difference between the Δ and the nucleon, $\Delta m_{\Delta N}$, due to the influence of the external magnetic field. We find that $\Delta m_{\Delta N}$ increases as the strength of the magnetic field grows.

PACS numbers: 12.39. Dc, 12.39. Fe, 12.40.Yx, 14.20.Dh

Keywords: Effective chiral Lagrangians, skyrmions, the strong magnetic field, the nucleon, the delta isobar

I. INTRODUCTION

Understanding how hadrons are modified in the presence of various external fields is an important topic in contemporary physics of hadrons. In particular, it is of great interest to investigate how the nucleon undergoes change in a strong magnetic field, since it provides certain information on both compact astrophysical objects and ultra-relativistic heavy-ion collision (URHIC), which unveils the nature of matter in the early Universe. A very strong magnetic field may exist in a magnetar in which the magnetic field reaches an order of $B_M \sim (10^{11} - 10^{15})$ G [1, 2]¹. Even stronger magnetic fields ($\sim 10^{16}$ to 10^{17} G) may be found in the cosmological γ -ray bursts [3, 4]. However, one can create even much stronger magnetic fields in the course of relativistic heavy-ion collisions [5]. At the Relativistic Heavy-Ion Collider (RHIC), the magnetic field could reach $B_M \sim 3 \times 10^{18}$ G and it may even rise to $B_M \sim 10^{19}$ G at the Large Hadron Collider (LHC) [6–14]. Although such an extremely strong magnetic field exists only during a very short period of time, it may bring about the distortion of hadrons and may change their properties greatly.

There has been already a great deal of theoretical works on modifications of hadrons under the influence of strong magnetic fields [15–29]. However, while they mainly concentrate on the modification of light and heavy meson properties in the presence of the strong magnetic fields, there are only few works on the changes of properties of the nucleon [29, 30]. Since Refs. [29, 30] aim at

describing the neutron stars, they focus only on the modification of the neutron in the strong magnetic fields. In the present work, we will investigate the modifications of the nucleon and Δ isobar properties in the presence of the strong magnetic fields within the framework of a chiral soliton approach.

The approach provides a simple but effective way of describing the structure of the nucleon. The main idea arises from the seminal papers by Witten [31–33]. In the limit of $N_c \rightarrow \infty$ (N_c as the number of colors), the mass of the nucleon is proportional to N_c whereas its width is of order $\mathcal{O}(1)$, which indicates that the meson fluctuations can be neglected. In this picture, a baryon arises as a topological chiral soliton that is called skyrmion [34, 35]. The nucleon as a chiral soliton is naturally an extended object, so that one can examine how the nucleon undergoes changes when a very strong magnetic field is exerted on it. A theoretical method has been developed over years, the environment surrounding the nucleon being treated collectively. It has been successfully applied to the description of the nucleon in nuclear medium [36–41], the nucleon in finite nuclei [42], the properties of nuclear matter [43] and even to the explanation of properties of atomic nuclei [44, 45]. The similar theoretical tool can be utilized for describing the nucleon in the strong magnetic field.

From a technical point of view, the nucleon in an external magnetic field is very similar to the situation when a skyrmion is embedded into an isospin asymmetric nuclear environment [43]. In general, one may expect that the magnetic field will change the nucleon properties less than the effects of isospin symmetry breaking. However, when it comes to the very strong magnetic fields that reach the level of URHICs at the LHC, the effects from the magnetic fields may become sizable. In this case, they may also play a crucial role in describing the evolution

* yakhshiev@inha.ac.kr

† hchkim@inha.ac.kr

‡ oka@post.j-parc.jp

¹ Here B_M denotes the strength of a magnetic field.

of the universe at an early stage [46, 47]. Moreover, such strong magnetic fields will reveal certain novel features relevant to the structure of the nucleon.

Depending on a specific configuration of the external magnetic field, one may further expect possible nonspherical deformations of the skyrmion in isospin and ordinary spaces [42, 44, 45] from the spherically symmetric *hedgehog* form corresponding to the skyrmion in free space [35, 48]. In this sense, the situation becomes even more interesting if the nucleon properties are studied in the presence of external isospin asymmetric nuclear environment that actually creates the strong magnetic field, that is, if the nucleon is located inside compact stellar objects in the presence of strong magnetic fields. The corresponding investigation can naturally be performed by generalizing the approach developed in Refs. [42–45] in the presence of an additional external magnetic field. However, we will concentrate only on the external magnetic field for simplicity and leave more general and complex studies as future works.

In the present work, we consider the homogenous magnetic field oriented along the axis of quantization. This choice allows us to consider axially symmetric solutions of the classical equation of motion for the soliton instead of a complicated situation where the soliton has totally an asymmetric form. Then we can employ the technique developed already for asymmetric nuclear environment [42, 44, 45]. Nevertheless, it is necessary to note that in the present work there will be some differences at the Lagrangian level due to the nature of the external magnetic field influencing the properties of the nucleon under consideration. In Refs. [42, 44, 45] the effect of environment on the skyrmion properties was introduced by means of the density functions, based on phenomenological information taken from mesonic atoms at low densities. Further modifications were achieved by introducing another density functions into the Lagrangian and relating them to the properties of nuclear matter near the saturation point $\rho_0 \approx 0.16 \text{ fm}^{-3}$ [43]. In the present work, the external magnetic field will be introduced by taking into account the U(1) gauge field into the original effective chiral Lagrangian [49].

The present paper is organized as follows: In the next Section II, we briefly discuss the Lagrangian of the model and the axially symmetric ansatz for the solutions of field equations. In Section III, we explain the variational method for the problem and discuss the parametrizations of profile functions. We also discuss the minimization process and present the classical results. Then we discuss how the baryon charge distribution is changed to a spheroidal form under the influence of the magnetic field. In Section IV, we show how to quantize the spheroidal skyrmion and discuss the changes of the nucleon properties in the magnetic field. In the last Section V we summarize the present results, draw conclusions, and give future outlook. The explicit expressions of the mass functional and the moments of inertia of the spheroidal skyrmion can be found in Appendix A.

II. LAGRANGIAN AND ANSATZ

We start with the effective chiral Lagrangian, incorporating explicit chiral symmetry breaking [48]

$$\mathcal{L} = -\frac{F_\pi^2}{16} \text{Tr} L_\mu L^\mu + \frac{1}{32e^2} \text{Tr}[L_\mu, L^\nu]^2 + \frac{F_\pi^2 m_\pi^2}{16} \text{Tr}[U + U^\dagger - 2], \quad (1)$$

where the first term is called the Weinberg term and the second one was originally introduced by Skyrme [34], which is also known as the Gasser-Leutwyler term in the large N_c . The chiral current L_μ is defined as $L_\mu = U^+ \partial_\mu U$, where the SU(2) unitary matrix $U = \exp\{2i\tau_a \pi_a / F_\pi\}$ is expressed in terms of the Cartesian isospin-components of the pion field π_a ($a = 1, 2, 3$). τ^a stand for the Pauli matrices in isospin space. There are three input parameters, i.e. the pion decay constant $F_\pi = 108.783 \text{ MeV}$, the skyrme parameter $e = 4.854$, and the pion mass $m_\pi = 134.977 \text{ MeV}$, which are chosen in such a way that the model properly reproduces the experimental data on the masses of the proton and neutron with breakdown of isospin symmetry taken into account (for the details, see Refs. [44, 45]).

In order to consider the effects of the external magnetic field we introduce the U(1) gauge field into the Lagrangian of Eq.(1). So, the ordinary derivative is replaced by the covariant one given in the form of

$$D_\mu U = \partial_\mu U + iq_e A_\mu [Q, U], \quad (2)$$

where q_e denotes the electric charge and A_μ stands for the electromagnetic four-vector potential (for example, see Ref.[50]). Here the charge operator in the SU(2) framework is defined as

$$Q = \frac{1}{6} \mathbb{I} + \frac{1}{2} \tau_3. \quad (3)$$

As mentioned above, we introduce the homogeneous magnetic field along the quantization axis or the z direction $\mathbf{B}_M = (0, 0, B_M)$, so we fix correspondingly the gauge of A^μ as follows

$$A^\mu = \left(0, -\frac{1}{2} y B_M, \frac{1}{2} x B_M, 0 \right). \quad (4)$$

When the magnetic field is absent, the hedgehog ansatz is imposed to be a spherically symmetric hedgehog form $U = \exp\{i\boldsymbol{\tau} \cdot \mathbf{n} P(\mathbf{r})\}$, where the unit vector in isospin space is chosen as a normal vector \mathbf{n} in ordinary three dimensional space. However, the ansatz for the skyrmion in the presence of the magnetic field may be deformed in the isospin and ordinary spaces deviating from the original spherical form in the absence of external fields. The most general form of the ansatz, which takes into account all possible deformations, can be represented as

$$U(\mathbf{r}) = \exp\{i\boldsymbol{\tau} \cdot \mathbf{N}(\mathbf{r}) P(\mathbf{r})\} \quad (5)$$

where the normal vector in isospin space is expressed as

$$\mathbf{N} = \begin{pmatrix} \sin \Theta(r, \theta, \varphi) \cos \Phi(r, \theta, \varphi) \\ \sin \Theta(r, \theta, \varphi) \sin \Phi(r, \theta, \varphi) \\ \cos \Theta(r, \theta, \varphi) \end{pmatrix} \quad (6)$$

in terms of two profile functions, $\Theta(r, \theta, \varphi)$ and $\Phi(r, \theta, \varphi)$. These two profile functions and $P(r, \theta, \varphi)$ describing the spatial extent of the pion fields will depend on all three (radial, polar and azimuthal) variables². Since we choose the magnetic field along the z direction, we have an axial symmetry, so the profile functions P and Θ become independent of the azimuthal angle φ , and the third profile function Φ can be selected as φ . Thus, one has the following axially symmetric ansatz

$$P = P(r, \theta), \quad \Theta = \Theta(r, \theta), \quad \Phi = \varphi \quad (7)$$

which will be used in the present work.

III. CLASSICAL SOLITON MASS AND PARAMETRIZATIONS OF PROFILE FUNCTIONS

Using the configuration given in Eqs. (5)-(7), one can find the mass of the static soliton M in the presence of the static magnetic field \mathbf{B}_M along the z direction. The mass functional $M[P, \Theta]$ is explicitly written by Eq. (A.2) in Appendix A. The field equations of the soliton can be derived by variation of M with respect to P and Θ . Since their expressions are rather lengthy and will not be used here, we will not present them in this work. In fact, they are coupled second-order partial differential equations of the following type³

$$\begin{aligned} g(P_{rr}, P_{\theta\theta}, P_r, P_\theta, \Theta_r, \Theta_\theta, P, \Theta) &= 0, \\ h(\Theta_{rr}, \Theta_{\theta\theta}, \Theta_r, \Theta_\theta, P_r, P_\theta, \Theta, P) &= 0, \end{aligned}$$

and the boundary conditions are determined by the baryon number, i.e. $B = 1$ in the present work. The baryon number of the axially deformed hedgehog configuration is given by the following expression

$$B = -\frac{1}{\pi} \int_0^\infty dr \int_0^\pi d\theta (P_r \Theta_\theta - P_\theta \Theta_r) \sin^2 P \sin \Theta. \quad (8)$$

Since we will use the variational method developed in Ref. [44], we will not write the explicit expression of the solitonic field equations, as mentioned previously. This will simplify all unnecessary technical complexities.

However, in order to clarify the form of trial functions to be used for a minimization process, let us for the moment ignore the nonspherical deformation effects and assume that the soliton has a spherical form even if it is

affected by the magnetic field. Then the equation of motion becomes an ordinary but nonlinear differential equation. For our purpose, we will rather concentrate on its linear approximation ($r \rightarrow \infty$) that yields the following form

$$\begin{aligned} P''(r) + \frac{2}{r} P'(r) - \frac{2}{r^2} P(r) \\ - \left(m_\pi^2 + \frac{2}{3} q_e B_M \right) P(r) - \frac{2}{15} (q_e B_M r)^2 P(r) = 0 \end{aligned} \quad (9)$$

Note that the last two terms contribute differently, depending on whether the magnetic field is strong or weak. They will bring about interesting consequences and will play a key role in understanding the present results later.

In general, Eq. (9) has a gaussian form of the solution

$$\begin{aligned} P(r) \sim \frac{1}{2^{1/4} r^2} \exp \left\{ -\frac{q_e B_M r^2}{\sqrt{30}} \right\} \\ \times U \left(\frac{-3 + \sqrt{30}}{12} + \frac{\sqrt{30} m_\pi^2}{8 q_e B_M}, -\frac{1}{2}; \sqrt{\frac{2}{15}} q_e B_M r^2 \right), \end{aligned} \quad (10)$$

where $U(a, b; c)$ is the confluent hypergeometric function of the second type. However, if $m_\pi^2 \gg q_e B_M$, then one can ignore the quadratic term in B_M of Eq. (9), keeping in mind that the soliton is localized at the finite region, i.e. even if r is large, the last term in Eq. (9) is not important due to the localization of solution. Then the corresponding solution takes the Yukawa-type form

$$P(r) \sim \frac{1 + Ar}{r^2} e^{-Ar}, \quad A = (m_\pi^2 + \frac{2}{3} q_e B_M)^{1/2}. \quad (11)$$

We will return to the consequences arising from these two different behaviors of the solutions, when we discuss the results. Having analyzed the characteristics of the solutions at this stage, we are able to choose the most appropriate forms of the trial profile functions P and Θ .

As a result, we can apply the following approximations for the spheroidal solutions

$$\begin{aligned} P(r, \theta) &= 2 \arctan \left\{ \frac{r_0^2}{r^2} (1 + Ar) [1 + u(\theta)] \right\} \\ &\times \exp \left\{ -\beta_0 Ar - \beta_1 q_e B_M r^2 \right\}, \end{aligned} \quad (12)$$

$$\Theta(r, \theta) = \theta + \zeta(r, \theta), \quad (13)$$

where r_0 , β_0 and β_1 are variational parameters. The functions u and ζ satisfy the inequalities $|u| < 1$ and $|\zeta| < 1$ in the regions $r \in [0, \infty)$ and $\theta \in [0, \pi]$. Thus, the trial function in Eq. (12) correctly reproduces the asymptotic forms of the solutions for both the weak and strong magnetic fields, and provides the smooth transitions between these two different cases. Furthermore, following the ideas of Ref. [42], we use for the function u the following parametrization

$$u(\theta) = q_e B_M \sum_{n=1}^{\infty} \gamma_n \cos^n \theta, \quad (14)$$

² In the present work we perform all calculations in the spherical coordinate system.

³ For the definitions of F_r , Θ_θ etc., see Appendix A.

where the set $\{\gamma_n\}$ consists of variational parameters in addition to those three mentioned previously. In the parametrization of Eq. (14), the cosine functions are chosen to maintain the periodicity in θ . Similarly, ζ can be selected as

$$\zeta(r, \theta) = q_e B_M r e^{-\delta_0^2 r^2} \sum_{n=1}^{\infty} \delta_n \sin(2n\theta), \quad (15)$$

where the set $\{\delta_n\}$ contains the remaining part of all the variational parameters in the present work. The prefactor ‘ $q_e B_M$ ’ in Eqs. (14) and (15) is introduced from the proper limiting consideration and will smoothen the variational process.

Note that the arguments of the sine functions in Eq. (15) are picked out to be a multiple of 2θ in order to avoid singularities given in the form ‘ $\sin \Theta / \sin \theta$ ’, which can be found in the mass functional $M[P, \Theta]$. Furthermore, the r dependence of ζ is singled out such that the equalities $\Theta(0, \theta) = \theta$ and $\Theta(\infty, \theta) = \theta$ are reproduced correctly. The mass functional will be easily extremized in terms of the trial functions given in Eqs. (12)-(15), and $B = 1$ condition will be naturally satisfied.

We want to mention that, in order to keep the minimization process with high accuracy, it is enough to consider only few terms in the trial functions (14) and (15). Furthermore, the current situation is in a more symmetric level than the case in which the nucleon is located in a finite nucleus at a given distance from its center. More specifically, when the nucleon is located inside the finite nucleus, the values of the profile functions P and Θ with the polar angle given in $\theta \in [0, \pi/2]$ are different from those with $\theta \in [\pi/2, \pi]$. This is due to the fact that the external field, which is expressed by the density distribution function of the external system, depends on the radial distance from the center of the nucleus (see Ref. [44]). On the other hand, the present case is symmetric under the change of the polar angles from $\theta \in [0, \pi/2]$ to $\theta \in [\pi/2, \pi]$, because the external magnetic field is homogeneously exerted along the z direction. Therefore, the symmetry in the polar angle brings about $\gamma_{2n-1} = 0$ ($n = 1, 2, \dots$) among $\{\gamma_n\}$ in Eq. (14).

The present variational approach is rather accurate, because both the solutions near the origin ($r \rightarrow 0$) and asymptotic region ($r \rightarrow \infty$) are properly given. The variational parameters introduced above connect smoothly the solution near the origin with the asymptotic one. For example, in the case of a free nucleon, we obtain almost the same results by either using the variational approach or directly solving the differential equations. Both the results differ within 1% (e.g. see Table 1 of Ref. [44]). In the present work, the same level of high accuracy is achieved.

Figure 1 draws the results for the change of the classical soliton mass due to the external magnetic field, i.e. $M(B_M) - M(0)$, where $M(B_M)$ and $M(0)$ denote respectively the values of the mass obtained with and without the magnetic field exerted. The mass of the classical soliton remains constant till the strength of the magnetic

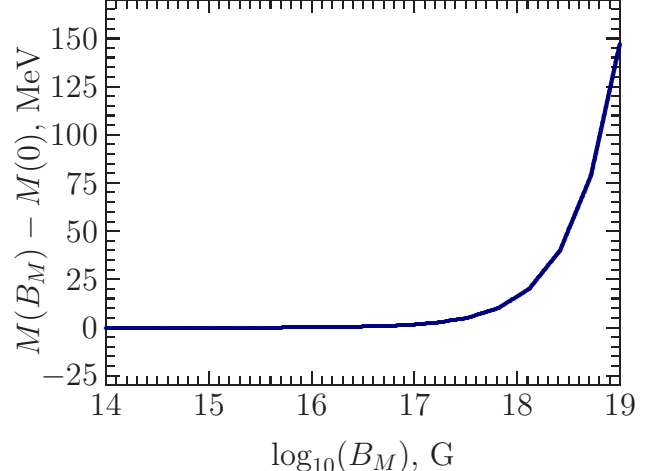


FIG. 1. (Color online) The change of the classical soliton mass as a function of the external magnetic field given in the log scale. $M(B_M)$ and $M(0)$ denote respectively the values of the mass obtained with and without the magnetic field exerted.

field reaches around 10^{17} G. However, as the magnetic field gets stronger than 10^{17} G, the value of the soliton mass starts to increase slowly till $B_M \approx 10^{18}$ G. If one raises the magnitude of the magnetic field, then the soliton mass starts to rise rather rapidly. When the magnitude of the magnetic field becomes 10^{19} G, the soliton mass acquires approximately additional 150 MeV by the external magnetic field.

Before we discuss the main results of the present work, we want to examine the values of the variational parameters for the profile functions. In Table I, we list their numerical results determined at the several selected values of the magnetic field. Among the parameters pre-

TABLE I. Variational parameters for the profile functions P and Θ at some selected values of the external magnetic field B_M .

B_M	0	10^{15} G	10^{17} G	10^{19} G
r_0 , fm 2	0.95646	0.95641	0.95200	0.97324
β_0	1.31568	1.31554	1.30447	0.93320
β_1	0	0	0	0.21958
γ_2 , fm 2	0	-0.64430	0.12305	0.33700
γ_4 , fm 2	0	0.30370	0.21985	0.08227
γ_6 , fm 2	0	-0.10019	-0.14775	0.21615
δ_0 , fm $^{-2}$	4.23604	3.90049	2.84256	3.21149
δ_1 , fm	0	0.13997	0.09016	0.9366
δ_2 , fm	0	0.24411	0.00207	0.00174

sented in Table I, nonzero values of γ_n ’s are responsible for the deviation of the P equi-surfaces from the spherical form, whereas δ_n ’s ($n > 0$) exhibit how the shape of the profile function is distorted from the spherically symmetric hedgehog form. One can see from Table I that at $B_M = 10^{15}$ G, which characterizes the strength of the magnetic fields in magnetars, the P equi-surfaces

already deviate from the spherically symmetric form.

It is interesting to observe that the value of β_1 is almost intact even at the upper limit of the strength of the magnetic fields in neutron stars ($\sim 10^{17}$ G). However, if the strength of the magnetic field gets stronger, then its value is not zero anymore (see the corresponding value listed in the last column of Table I for $B_M = 10^{19}$ G). In order to understand this behavior, we need to scrutinize the exponential term in Eq. (12). When A in the first term is much larger than $(rq_e B_M)^2$ in the second one, for example, when $r^2 (q_e \times 10^{17} \text{ G})^2 \sim 10 \text{ MeV}^2 \ll (m_\pi^2 + 2q_e B_M/3) \approx m_\pi^2 \sim 0.18 \text{ GeV}^2$ numerically, then the asymptotic solution is not much influenced by the second term for the typical soliton size ($r \sim 1 \text{ fm}$). However, when the magnetic field is extremely strong, i.e. $B_M \sim 10^{19}$ G, we find $q_e B_M > m_\pi^2$. Thus, the second term dominates over the first one. It implies that the profile $P(r, \theta)$ will be shrunken by the second Gaussian term and β_1 is not zero anymore.

To understand the above-mentioned nature more clearly, we will delve into the baryon charge distribution of the axially deformed skyrmion, which is expressed as⁴

$$B_0(r, \theta) = -\frac{P_r \Theta_\theta - P_\theta \Theta_r}{2\pi^2 r^2} \left(\frac{\sin \Theta}{\sin \theta} \right) \sin^2 P. \quad (16)$$

It will explicitly reveal how the soliton undergoes deformation in the presence of the strong magnetic field. In the left panel of Fig. 2, we depict the profiles of the baryon charge distributions along the z direction ($\theta = 0$), while the right panel of Fig. 2 draws those in the perpendicular plane to the z axis ($\theta = \pi/2$). Dotted curves correspond to the results with $B_M = 0$, which should be spherically symmetric and are the same in both the left and right panels. We can take them as a reference for comparison. Taking the value of the magnetic field to be $B_M = 10^{17}$ G, we see that the charge distribution of the soliton along the z direction is deformed slightly, whereas it remains the same as that in the absence of magnetic field as shown in the right panel. If we take $B_M = 10^{19}$ G, which can be realized in URHICs at the LHC, then the baryon charge distribution displays evidently the deformation of the soliton both along the z direction and in the perpendicular plane to it.

To illuminate how the baryon charge distribution undergoes the change as the strength of the magnetic field is varied, we define the *anisotropy of the baryon charge distribution* as

$$\Delta B_0(r) \equiv B_0(r, \pi/2) - B_0(r, 0), \quad (17)$$

where $B_0(r, \pi/2)$ represents the baryon charge distribution in the perpendicular plane to the z axis, and $B_0(r, 0)$ denotes that along the z direction. Equation (17) shows

how the isotropy of the baryon charge distribution is broken by the magnetic field. In Fig. 3 we illustrate, respectively, the results of ΔB_0 as functions of r in the left panel and those at $r = 0.2 \text{ fm}$ as a function of the magnetic field in the right panel. The results in the left panel of Fig. 3 clearly show that when $B_M = 10^{17}$ G, which corresponds to the dashed curve, the soliton is more deformed along the z direction than in the perpendicular plane to it. Moreover, it mainly occurs in the core part of the soliton. It implies that the baryon charge distribution will be taken slightly as a cigar-type form, since the results of $\Delta B_0(r)$ decreases in the core part. If one takes the stronger value of the magnetic field, i.e. $B_M = 10^{19}$ G, then the baryon charge distribution is drastically changed from the previous case of $B_M = 10^{17}$ G. The core part of the soliton undergoes the deformation in the xy plane more strongly than along the z direction. On the other hand, when it comes to its peripheral part, the situation is reversed. That is, while the peripheral shape of the soliton is less distorted than in the core part, the soliton is slightly more deformed along the z direction in comparison with that in the perpendicular plane to it.

To see the process of the soliton deformation more closely, we scrutinize ΔB_0 at a fixed value of r , for example, at $r = 0.2 \text{ fm}$, as the B_M field varied from 10^{17} G to 10^{19} G. The corresponding result is illustrated in the right panel of Fig. 3. When the strength of the magnetic field is given between 10^{17} G and 10^{18} G, we can clearly observe that the core part of the soliton is more deformed in the xy plane, compared with that along the z direction. However, if we further increase the strength of the magnetic field close to 10^{19} G, the situation becomes other way around, i.e. the core part of the soliton is deformed more strongly along the z direction in comparison with that in the perpendicular plane to it.

In general, the baryon charge distribution is more compactly deformed in the presence of the strong magnetic field. This can be observed by comparing the solid curves with dotted ones in both the panels of Fig. 2. Since the quadratic term with regards to B_M in Eq. (12) come into dominant play when the magnetic field is very strong. In fact, this is related to the quadratic term like a harmonic oscillator potential in the approximated differential equation given in Eq. (9) in the asymptotic limit, which plays effectively a role of a confining potential that arises from the the strong magnetic field. The physical implications of this confining potential are that the charged pions are localized and are forced to be confined by the external strong magnetic field.⁵ We can examine this localization by considering the baryon charge distribution within a certain region. For example, we integrate the baryon

⁴ See Eq. (8) above.

⁵ Here, we remind that the baryon is a topological object made of the nonlinearly interacting pions.

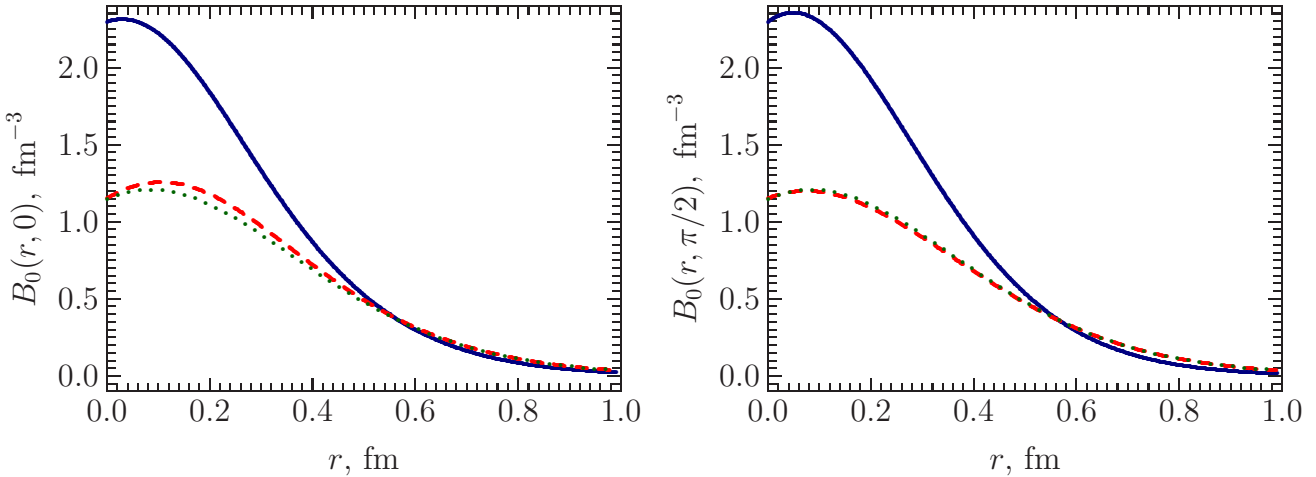


FIG. 2. (Color online) Results of the baryon charge distributions along the z direction (left panel) and in the perpendicular plane to the z axis (right panel), respectively. The solid curves depict the results with $B_M = 10^{19}$ G, the dashed ones draw those with $B_M = 10^{17}$ G, and the dotted ones correspond to the case of $B_M = 0$, respectively.

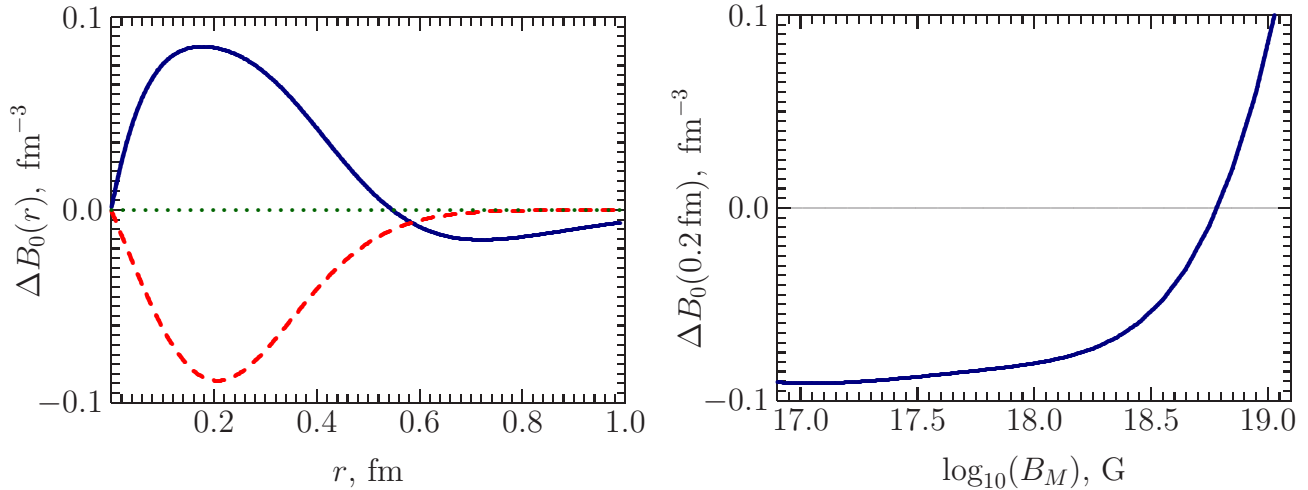


FIG. 3. (Color online) The left panel draws the results of the anisotropy $\Delta B_0(r)$ defined in Eq. (17) as functions of r , whereas the right panel shows the result of $\Delta B_0(0.2 \text{ fm})$ fixed at $r = 0.2 \text{ fm}$ as a function of the magnetic field. Notations in the left panel are the same as in Fig. 2.

charge distribution up to 1 fm

$$B_{(1 \text{ fm})} = \int_0^{1 \text{ fm}} r^2 dr \int d\Omega B_0 \quad (18)$$

with the magnetic field varied. Then, comparing the results with different values of B_M , we can see how the charged pions are forced toward the core region inside a nucleon. Taking three different values of B_M , we obtain the following results: $B_{(1 \text{ fm})} = 0.9014$ for $B_M = 0$, $B_{(1 \text{ fm})} = 0.9024$ for $B_M = 10^{17}$ G and $B_{(1 \text{ fm})} = 0.9665$ for $B_M = 10^{19}$ G, respectively⁶. The comparison of these

values indicates that the baryon charge distribution is indeed squeezed into the core region due to the localization of the charged pions.

IV. QUANTIZATION OF THE SPHEROIDAL SOLITON

We are now in a position to discuss the quantization of the axially deformed soliton, i.e., the spheroidal one and the relevant results. The quantization of a spherically symmetric chiral soliton is generally performed by introducing the zero-mode quantization with the collective coordinates introduced [35]. As we already discussed in the previous Section, the spherical symmetry of the soliton is already broken in the presence of the magnetic

⁶ Of course, we get $B = 1$ in all cases if one integrates properly all over the region, as must happen.

field. However, we still have an axial symmetry as presented in Eqs. (5)-(7). Thus, we consider independent rotations in the coordinate and isospin spaces as follows

$$P = P(\mathcal{R}^{-1}(t)\mathbf{r}), \quad \mathbf{N} = \mathcal{I}(t)\mathbf{N}(\mathcal{R}^{-1}(t)\mathbf{r}), \quad (19)$$

where \mathcal{R} and \mathcal{I} represent the SO (3) rotational and iso-rotational matrices, respectively. Having carried out these slow time-dependent rotations and performed the spatial integration, we arrive at a collective Lagrangian

$$\begin{aligned} L = & -M + \frac{\omega_1^2 + \omega_2^2}{2} \Lambda_{\omega\omega,12} - (\omega_1 \Omega_1 + \omega_2 \Omega_2) \Lambda_{\omega\Omega,12} \\ & + \frac{\Omega_1^2 + \Omega_2^2}{2} \Lambda_{\Omega\Omega,12} + \frac{(\omega_3 - \Omega_3)^2}{2} \Lambda_{\omega\Omega,33}. \end{aligned} \quad (20)$$

Here ω_i and Ω_i denote the angular velocities in isospin and coordinate spaces, respectively. The explicit expressions of the functionals $\Lambda[P, \Theta]$ can be found in Appendix A.

Defining the canonical conjugate variables in the body-fixed reference system as

$$T_i = \frac{\partial L}{\partial \omega_i} \quad \text{and} \quad J_i = \frac{\partial L}{\partial \Omega_i}, \quad (21)$$

we derive from the time-dependent Lagrangian in Eq. (20) the collective Hamiltonian as

$$\begin{aligned} \hat{H} = & M + \frac{\hat{T}_3^2}{2\Lambda_{\omega\Omega,33}} + \frac{(\hat{T}_1\hat{J}_1 + \hat{T}_2\hat{J}_2)\Lambda_{\omega\Omega,12}}{\Lambda_{\omega\omega,12}\Lambda_{\Omega\Omega,12} - \Lambda_{\omega\Omega,12}^2} \\ & + \frac{(\hat{T}_1^2 + \hat{T}_2^2)\Lambda_{\Omega\Omega,12} + (\hat{J}_1^2 + \hat{J}_2^2)\Lambda_{\omega\omega,12}}{2(\Lambda_{\omega\omega,12}\Lambda_{\Omega\Omega,12} - \Lambda_{\omega\Omega,12}^2)}. \end{aligned} \quad (22)$$

Diagonalizing the Hamiltonian of Eq. (22), we obtain the baryon eigenstates $|T, T_3; J, J_3\rangle$ and the energies of the axially deformed nucleon and the Δ isobar:

$$\begin{aligned} E = & M + \frac{T_3^2}{2\Lambda_{\omega\Omega,33}} \\ & + \frac{\Lambda_{\Omega\Omega,12} + \Lambda_{\omega\omega,12} - 2\Lambda_{\omega\Omega,12}}{2(\Lambda_{\omega\omega,12}\Lambda_{\Omega\Omega,12} - \Lambda_{\omega\Omega,12}^2)} (T(T+1) - T_3^2). \end{aligned} \quad (23)$$

From the third term of Eq. (23), one observes that in the presence of the external magnetic field the degeneracy in the energy between the different isospin states of the Δ isobar are partially lifted. For example, the proton and neutrons are still in degeneracy, i.e. $m_p = m_n$, while the Δ isobar isospin states are partially split, i.e. $m_{\Delta^{++}} = m_{\Delta^-} \neq m_{\Delta^+} = m_{\Delta^0}$.

The results for the masses of baryons at certain values of the magnetic field B_M are listed in Table II. As in the case of the classical soliton, the masses of the nucleons and Δ isobars are almost intact till the strength of the magnetic field is reached at around 10^{17} G. Keeping in mind that the magnetic field in magnetars is approximately $B_M = 10^{15}$ G, the baryon masses are almost not changed. However, if one further increases the

TABLE II. Masses of baryons at some selected values of the external magnetic field B_M . All masses are given in units of MeV.

B_M	0	10^{15} G	10^{17} G	10^{19} G
$m_{n,p}$	939.8035	939.8212	941.5769	1113.4133
m_{Δ^{++},Δ^-}	1233.6770	1233.6951	1236.5624	1530.4224
m_{Δ^+,Δ^0}	1233.6770	1233.6949	1236.3618	1507.7573

strength of B_M , the masses of all the nucleons and Δ isobars start to grow. At $B_M = 10^{17}$ G the change of the baryon mass is already not negligible. Then, when it is reached to $B_M = 10^{19}$ G, the masses increase by about 15–20 %. Note that Δ -isobar states actually remain degenerate even though the magnetic field gets very strong. Only at very large values of the magnetic field, the degeneracy of the Δ isobars will be partially lifted as discussed above.

In Fig. 4 we show how the masses of the baryons will be changed as B_M increases. The results look very sim-

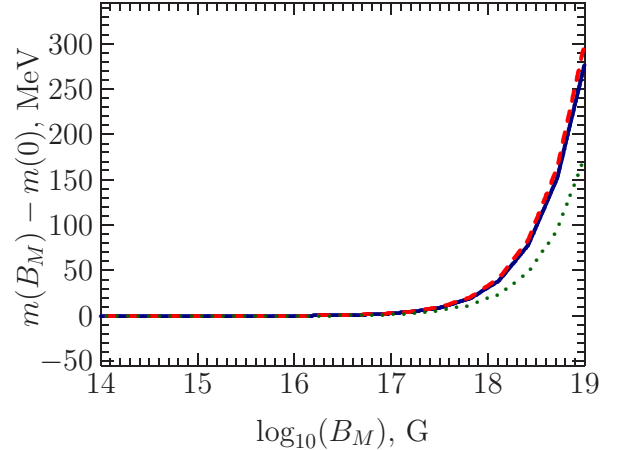


FIG. 4. (Color online) The changes of the baryon masses as a function of the magnetic field. The solid curve depicts m_{Δ^0} , whereas the dashed one draws m_{Δ^-} . The dotted one represents m_n , respectively.

ilar to the change of the classical soliton mass as shown in Fig. 1. However, the rates of the increment in the masses of the baryons are still different. The reason can be found in the changes of the moments of inertia⁷. Since the soliton is deformed in the presence of the strong magnetic fields, the magnitudes of the moments of inertia are decreased. It indicates that not only the baryon charge distribution is changed but also the mass distribution inside the soliton becomes more compact in the presence of the strong magnetic field than in free space. As was done in the case of the baryon charge distribution, we can consider the integrate value of the mass distribution

⁷ The formulae for the moments of inertia, see Eq. (A.5).

up to 1 fm (see Eq. (18)). Then we obtain the results at three different values of B_M as follows: $M_{(1\text{ fm})} = 0.818M$ for $B_M = 0$, $M_{(1\text{ fm})} = 0.820M$ for $B_M = 10^{17}\text{ G}$ and $M_{(1\text{ fm})} = 0.911M$ for $B_M = 10^{19}\text{ G}$. This indicates that the masses of the baryons tend to be more compact in the presence of the magnetic fields than in free space.

It is also very interesting to examine the moments of inertia for the spheroidal solitons. We first define the following quantities

$$\Delta m_{(0,-)}(B_M) = [m_{\Delta^0}(B_M) - m_{\Delta^-}(B_M)] - [m_{\Delta^0}(0) - m_{\Delta^-}(0)], \quad (24)$$

$$\Delta m_{(0,n)}(B_M) = [m_{\Delta^0}(B_M) - m_n(B_M)] - [m_{\Delta^0}(0) - m_n(0)], \quad (25)$$

$$\Delta m_{(-,n)}(B_M) = [m_{\Delta^-}(B_M) - m_n(B_M)] - [m_{\Delta^-}(0) - m_n(0)]. \quad (26)$$

They describe how much the mass splittings of the baryons undergo the changes in the presence of the magnetic field. The results are illustrated in Fig. 5. Here we

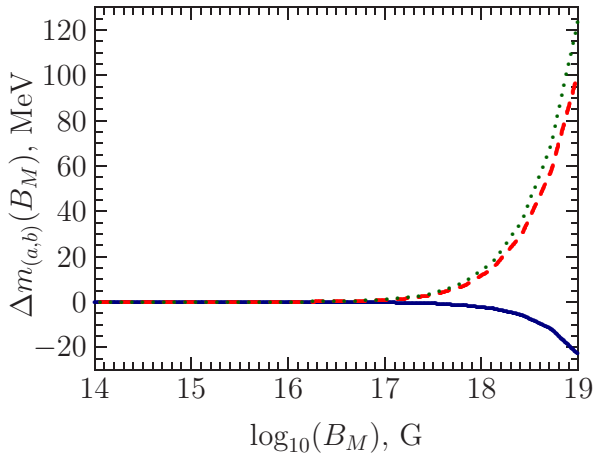


FIG. 5. (Color online) The change of the baryon mass splittings in the presence of the magnetic field. The solid curve draws the result of $\Delta m_{(0,-)}(B_M)$, whereas the dashed one depicts $\Delta m_{(0,n)}(B_M)$. The dotted one shows $\Delta m_{(-,n)}(B_M)$. For the definitions of $\Delta m_{(a,b)}$, see Eqs. (25)-(26).

explicitly demonstrate that the moments of inertia decrease, which bring about the rise of the $\Delta - N$ mass splittings, which are illustrated in the dashed and dotted curves in Fig. 5. One can also observe that the mass degeneracy in the different isospin states of the Δ isobars is lifted, as shown in the solid curve of Fig. 5. While the degeneracy is more or less kept to be intact till $B_M = 10^{17}\text{ G}$, it starts to be removed. If B_M continues to increase, the splitting between the Δ^0 and Δ^- masses becomes prominent.

Finally, we want to mention that there is still a caveat that is related to the strong magnetic fields. A novel feature emerges when the magnetic field is very strong, called the Pachen-Beck (PB) effect [51]. Originally, the PB effect arises when the strength of the magnetic field

dominates over the spin-orbit coupling of an atomic system. In the presence of the weak magnetic field, all the eigenstates of an atom are split, which is known as the anomalous Zeeman effect. However, if the magnetic field is so strong that it overcomes the spin-orbit interaction, then the spherical symmetry is completely broken, so that the total angular momentum squared, J^2 , is no more a good quantum number but L_z and S_z are the good quantum numbers [52]. However, we still have cylindrical symmetry or axial symmetry in the presence of the constant external magnetic field along a specific direction as discussed in this work. Thus, $2(2l+1)$ degeneracy in $m_l + m_s$ will appear. This is called the PB effect. In fact, Iwasaki et al. discussed the PB effect [53], when the strong magnetic field ($\sim 10^{19}\text{ G}$) is exerted on a charmonium system. They found a very interesting feature: The strong magnetic field induces mixings between $S = 0$ and $S = 1$ states. This may lead to the mixing between the η_c and J/ψ in $S = 1$ and $S_z = 0$ states. It implies that when the magnetic field is very strong, one can expect the same phenomena in a baryonic system such as the mixing between the proton with $S = 1/2$ and $S_z = 1/2$ and the Δ^+ isobar with $S = 3/2$ and $S_z = 1/2$. We will investigate this important physics elsewhere.

V. SUMMARY AND OUTLOOK

In the present work, we investigated how the nucleons and Δ isobars undergo the deformation in the presence of the strong magnetic field within the framework of the Skyrme model. We first examined the changes of the classical soliton under the influence of the strong magnetic field. The mass of the classical soliton remains unchanged till the magnitude of the magnetic field reached 10^{17} G . However, if the magnetic field gets stronger than this value, the mass starts to increase. The soliton is deformed in a rather nontrivial way as the strength of the magnetic field varied. We exhibited explicitly and thoroughly how the soliton properties were changed as the magnetic field was altered. When the magnitude of the magnetic field is 10^{17} G , the soliton was deformed more strongly along the z direction than in the perpendicular plane to it. The core part of the soliton was mainly modified, which indicates that the shape of the soliton will turn to a cigar-type form. If the value magnetic field was taken to be 10^{19} G , then the baryon charge distribution was drastically altered. The core part of the soliton was deformed more strongly in the xy plane than along the z direction. On the contrary, the peripheral shape of the soliton was less distorted than in the core part, whereas the soliton was slightly more deformed along the z direction than in the perpendicular plane to it.

We performed the zero-mode quantization of the spheroidal soliton in the presence of the magnetic field. We found that the solitonic moments of inertia decreases as the magnetic field increases. It means that the masses of the nucleon and Δ isobar should get larger. More-

over, we observed that Δ -N mass splitting also increases. The spherical nucleon in free space was deformed into a cigar-type form when the magnetic field was present. The case of the Δ isobars was similar to the nucleon case but their masses increased slightly more than the nucleon did as the magnetic field is strengthened. We found that the mass of Δ^{++} is degenerate with that of Δ^- , whereas Δ^+ has the same mass as Δ^0 . However, the mass degeneracy was partially lifted.

From the present work, we conclude that there is no need to consider the effects of the strong magnetic field in analyzing the equation of the states at high densities that may exist in interiors of compact stellar objects, since the nucleon masses are almost intact till the magnitude of the magnetic field reaches 10^{17} G. However, when it comes to ultra-relativistic heavy ion collisions at the LHC, it is of great significance to take into accounts the effects coming from the strong magnetic field. This will lead to nontrivial consequences. Furthermore, generalizations of the model may be performed by including the explicit isospin breaking effects in the mesonic sector in order to study the changes in the neutron-proton mass difference under the influence of the external magnetic field. The Paschen-Beck effects on baryonic systems are yet another interesting issue, which can be investigated as future works. The relevant works are under way.

ACKNOWLEDGMENTS

We are grateful to P. Gubler, A. Hosaka, K. Itakura, T. Maruyama for useful discussions. U.Y. and H.-Ch.K. would like to express their gratitude to the members of the Advanced Science Research Center at Japan Atomic Energy Agency for the hospitality, where the present work was done. This work is supported by the Basic Science Research Program through the National Research Foundation (NRF) of Korea funded by the Korean government (Ministry of Education, Science and Technology, MEST), No. 2016R1D1A1B03935053 (UY) and No. 2018R1A2B2001752 (HChK).

Appendix A: Mass and moments of inertia of the spheroidal soliton

For convenience, we introduce the following short-handed notations:

$$\begin{aligned} P_r &\equiv \partial_r P, \quad P_\theta \equiv \partial_\theta P, \quad \Theta_r \equiv \partial_r \Theta, \quad \Theta_\theta \equiv \partial_\theta \Theta, \\ S_P &\equiv \sin P, \quad C_P \equiv \cos P, \quad S_\Theta \equiv \sin \Theta, \\ C_\Theta &\equiv \cos \Theta, \quad s_\theta \equiv \sin \theta, \quad c_\theta \equiv \cos \theta. \end{aligned} \quad (\text{A.1})$$

The classical soliton mass M in the Lagrangian in Eq. (20) and the explicit change of the soliton mass ΔM

in the external magnetic field are expressed as follows:

$$\begin{aligned} M = \pi \int_0^\infty dr r^2 \int_0^\pi s_\theta d\theta &\left\{ \frac{F_\pi^2}{4r^2} \left[P_\theta^2 + r^2 P_r^2 \right. \right. \\ &+ S_P^2 \left(\frac{S_\Theta^2}{s_\theta^2} + \Theta_\theta^2 + r^2 \Theta_r^2 \right) \left. \right] \\ &+ \frac{S_P^2}{e^2 r^4} \left[\frac{S_\Theta^2}{s_\theta^2} (P_\theta^2 + r^2 P_r^2) \right. \\ &+ S_P^2 \frac{S_\Theta^2}{s_\theta^2} (\Theta_\theta^2 + r^2 \Theta_r^2) + r^2 (P_r \Theta_\theta - P_\theta \Theta_r)^2 \left. \right] \\ &+ \frac{m_\pi^2 F_\pi^2}{2} (1 - C_P) \left. \right\} + \Delta M, \end{aligned} \quad (\text{A.2})$$

$$\begin{aligned} \Delta M = \pi \int_0^\infty dr r^2 \int_0^\pi s_\theta d\theta &\left\{ \frac{F_\pi^2}{16} \right. \\ &+ \frac{1}{4e^2 r^2} (P_\theta^2 + r^2 P_r^2 + S_P^2 (\Theta_\theta^2 + r^2 \Theta_r^2)) \\ &\times q_e B_M (4 + q_e B_M r^2 s_\theta^2) S_P^2 S_\Theta^2. \end{aligned} \quad (\text{A.3})$$

The generic form for the moment of inertia is defined as

$$\Lambda = 2\pi \int_0^\infty dr r^2 \int_0^\pi s_\theta d\theta \lambda, \quad (\text{A.4})$$

where the contributions from the different parts of the Lagrangian (20) are given as

$$\begin{aligned} \lambda_{\omega\omega,12} = \Delta \lambda_{\omega\omega,12} &+ \frac{F_\pi^2}{8} (1 + C_\Theta^2) S_P^2 \\ &+ \frac{S_P^2}{2e^2 r^2} \left[(1 + C_\Theta^2) (P_\theta^2 + r^2 P_r^2) \right. \\ &+ S_P^2 \left(\frac{S_\Theta^2}{s_\theta^2} + C_\Theta^2 (\Theta_\theta^2 + r^2 \Theta_r^2) \right) \left. \right], \end{aligned} \quad (\text{A.5})$$

$$\begin{aligned} \lambda_{\omega\Omega,12} = \Delta \lambda_{\omega\Omega,12} &+ \frac{F_\pi^2}{8} \left(c_\theta C_\Theta \frac{S_\Theta}{s_\theta} + \Theta_\theta \right) S_P^2 \\ &+ \frac{S_P^2}{2e^2 r^2} \left[c_\theta C_\Theta \frac{S_\Theta}{c_\theta} \left(P_\theta^2 + r^2 P_r^2 \right. \right. \\ &+ S_P^2 (\Theta_\theta^2 + r^2 P_r^2) \left. \right) + S_P^2 S_\Theta^2 s_\theta^{-2} \Theta_\theta \\ &\left. + r^2 P_r (P_r \Theta_\theta - \Theta_r P_\theta) \right], \end{aligned} \quad (\text{A.6})$$

$$\begin{aligned} \lambda_{\Omega\Omega,12} = \Delta \lambda_{\Omega\Omega,12} &+ \frac{F_\pi^2}{8} \left[P_\theta^2 + S_P^2 \left(c_\theta^2 \frac{S_\Theta^2}{s_\theta^2} + \Theta_\theta^2 \right) \right] \\ &+ \frac{S_P^2}{2e^2 r^2} \left[\frac{S_\Theta^2}{s_\theta^2} \left((1 + c_\theta^2) (P_\theta^2 + S_P^2 \Theta_\theta^2) \right. \right. \\ &+ r^2 (P_r^2 + S_P^2 \Theta_r^2) c_\theta^2 \left. \right) \\ &\left. + r^2 (P_r \Theta_\theta - P_\theta \Theta_r)^2 \right], \end{aligned} \quad (\text{A.7})$$

$$\begin{aligned} \lambda_{\omega\Omega,33} = \frac{F_\pi^2}{4} S_\Theta^2 S_P^2 &+ \frac{S_P^2}{e^2 r^2} S_\Theta^2 \left(P_\theta^2 + r^2 P_r^2 \right. \\ &+ S_P^2 (\Theta_\theta^2 + r^2 \Theta_r^2) \left. \right). \end{aligned} \quad (\text{A.8})$$

Finally, the additional parts of the moments of inertia arising from the external magnetic field are expressed as

$$\Delta\lambda_{\omega\omega,12} = \frac{q_e B_M}{4e^2} (4 + q_e B_M r^2 s_\theta^2) S_P^4 S_\Theta^2, \quad (\text{A.9})$$

$$\Delta\lambda_{\omega\Omega,12} = \frac{q_e B_M}{4e^2} (4 + q_e B_M r^2 s_\theta^2) S_P^4 S_\Theta^2 \Theta_\theta, \quad (\text{A.10})$$

$$\begin{aligned} \Delta\lambda_{\Omega\Omega,12} = & \frac{q_e B_M}{4e^2} (4 + q_e B_M r^2 s_\theta^2) S_P^2 S_\Theta^2 \\ & \times (P_\theta^2 + S_P^2 \Theta_\theta^2). \end{aligned} \quad (\text{A.11})$$

[1] S. Mereghetti, J. Pons and A. Melatos, *Space Sci. Rev.* **191**, 315 (2015).

[2] V. M. Kaspi and A. Beloborodov, *Ann. Rev. Astron. Astrophys.* **55**, 261 (2017).

[3] C. Kouveliotou *et al.*, *Nature* **393**, 235 (1998).

[4] P. Bhattacharjee and G. Sigl, *Phys. Rept.* **327**, 109 (2000).

[5] J. Rafelski and B. Muller, *Phys. Rev. Lett.* **36**, 517 (1976).

[6] V. Skokov, A. Y. Illarionov and V. Toneev, *Int. J. Mod. Phys. A* **24**, 5925 (2009).

[7] X. G. Huang, *Rept. Prog. Phys.* **79**, 076302 (2016).

[8] D. E. Kharzeev, L. D. McLerran and H. J. Warringa, *Nucl. Phys. A* **803**, 227 (2008).

[9] V. Voronyuk, V. D. Toneev, W. Cassing, E. L. Bratkovskaya, V. P. Konchakovski and S. A. Voloshin, *Phys. Rev. C* **83**, 054911 (2011).

[10] L. Ou and B. A. Li, *Phys. Rev. C* **84**, 064605 (2011).

[11] J. Bloczynski, X. G. Huang, X. Zhang and J. Liao, *Nucl. Phys. A* **939**, 85 (2015).

[12] W. T. Deng and X. G. Huang, *Phys. Lett. B* **742**, 296 (2015).

[13] K. Hattori and X. G. Huang, *Nucl. Sci. Tech.* **28**, 26 (2017).

[14] X. L. Zhao, Y. G. Ma and G. L. Ma, *Phys. Rev. C* **97**, 024910 (2018).

[15] Y. Hidaka and A. Yamamoto, *Phys. Rev. D* **87**, no. 9, 094502 (2013).

[16] C. S. Machado, F. S. Navarra, E. G. de Oliveira, J. Noronha and M. Strickland, *Phys. Rev. D* **88**, 034009 (2013).

[17] J. Alford and M. Strickland, *Phys. Rev. D* **88**, 105017 (2013).

[18] C. S. Machado, S. I. Finazzo, R. D. Matheus and J. Noronha, *Phys. Rev. D* **89**, 074027 (2014).

[19] E. V. Luschevskaya, O. E. Solovjeva, O. A. Kochetkov and O. V. Teryaev, *Nucl. Phys. B* **898**, 627 (2015).

[20] H. Taya, *Phys. Rev. D* **92**, 014038 (2015).

[21] C. Bonati, M. D'Elia and A. Rucci, *Phys. Rev. D* **92**, 054014 (2015).

[22] P. Gubler, K. Hattori, S. H. Lee, M. Oka, S. Ozaki and K. Suzuki, *Phys. Rev. D* **93**, 054026 (2016).

[23] K. Suzuki and T. Yoshida, *Phys. Rev. D* **93**, 051502 (2016).

[24] E. V. Luschevskaya, O. A. Kochetkov, O. V. Teryaev and O. E. Solovjeva, *JETP Lett.* **101**, 674 (2015).

[25] M. A. Andreichikov, B. O. Kerbikov, E. V. Luschevskaya, Y. A. Simonov and O. E. Solovjeva, *JHEP* **1705**, 007 (2017).

[26] H. Liu, X. Wang, L. Yu and M. Huang, *Phys. Rev. D* **97**, no. 7, 076008 (2018).

[27] M. Coppola, D. Gómez Dumm and N. N. Scoccola, *Phys. Lett. B* **782**, 155 (2018).

[28] S. S. Avancini, R. L. S. Farias and W. R. Tavares, arXiv:1812.00945 [hep-ph].

[29] M. A. Andreichikov, B. O. Kerbikov, V. D. Orlovsky and Y. A. Simonov, *Phys. Rev. D* **89**, 074033 (2014).

[30] M. Bigdeli, *Phys. Rev. C* **95**, 024309 (2017).

[31] E. Witten, *Nucl. Phys. B* **160**, 57 (1979).

[32] E. Witten, *Nucl. Phys. B* **223**, 422 (1983).

[33] E. Witten, *Nucl. Phys. B* **223**, 433 (1983).

[34] T. H. R. Skyrme, *Proc. Roy. Soc. Lond. A* **260**, 127 (1961).

[35] G. S. Adkins, C. R. Nappi and E. Witten, *Nucl. Phys. B* **228**, 552 (1983).

[36] H.-Ch. Kim, P. Schweitzer and U. T. Yakhshiev, *Phys. Lett. B* **718**, 625 (2012).

[37] U. T. Yakhshiev and H.-Ch. Kim, *Phys. Lett. B* **726**, 375 (2013).

[38] J. H. Jung, U. T. Yakhshiev and H.-Ch. Kim, *Phys. Lett. B* **723**, 442 (2013).

[39] J. H. Jung, U. Yakhshiev, H.-Ch. Kim and P. Schweitzer, *Phys. Rev. D* **89**, no. 11, 114021 (2014).

[40] J. H. Jung, U. Yakhshiev and H.-Ch. Kim, *Phys. Rev. D* **93**, 054016 (2016).

[41] K. H. Hong, U. Yakhshiev and H.-Ch. Kim, arXiv:1806.06504 [nucl-th].

[42] U. T. Yakhshiev, M. M. Musakhanov, A. M. Rakhimov, U. G. Meissner and A. Wirzba, *Nucl. Phys. A* **700** (2002) 403 [nucl-th/0109008].

[43] U. T. Yakhshiev, *Phys. Rev. C* **88**, no. 3, 034318 (2013).

[44] U. G. Meissner, A. M. Rakhimov, A. Wirzba and U. T. Yakhshiev, *Eur. Phys. J. A* **36**, 37 (2008) [arXiv:0802.1455 [nucl-th]].

[45] U. G. Meissner, A. M. Rakhimov, A. Wirzba and U. T. Yakhshiev, *EPJ Web Conf.* **3**, 06008 (2010) [arXiv:0912.5170 [nucl-th]].

[46] G. Steigman, *Int. J. Mod. Phys. E* **15**, 1 (2006) [arXiv:astro-ph/0511534].

[47] R. H. Cyburt, *Phys. Rev. D* **70**, 023505 (2004) [arXiv:astro-ph/0401091].

- [48] G. S. Adkins and C. R. Nappi, Nucl. Phys. B **233**, 109 (1984).
- [49] J. Gasser and H. Leutwyler, Nucl. Phys. B **250**, 465 (1985). doi:10.1016/0550-3213(85)90492-4
- [50] T. E. Rudy, H. W. Fearing and S. Scherer, Phys. Rev. C **50**, 447 (1994) [hep-ph/9401302].
- [51] F. Paschen, E. Back, Physica **1**, 261 (1921).
- [52] J. J. Sakurai and J. Napolitano, *Modern quantum physics*, 2nd Ed., (Cambridge University Press, Cambridge UK, 2017)
- [53] S. Iwasaki, M. Oka, K. Suzuki and T. Yoshida, Phys. Lett. B **790**, 71 (2019).